Arabian Journal of Chemistry (2021) **14**, 103395

King Saud University

Arabian Journal of Chemistry

www.ksu.edu.sa
www.sciencedirect.com

ORIGINAL ARTICLE

Sulfamide-substituted-BODIPY based fluorescence drugs: Synthesis, spectral characteristics, molecular docking, and bioactivity

Feng Zhao [a], **Yuling Wang** [b], **Guofan Jin** [b,*]

[a] *Affiliated Hospital of Jiangsu University, Zhenjiang 212013, PR China*
[b] *School of Pharmacy, Jiangsu University, Zhenjiang 212013, PR China*

Received 21 June 2021; accepted 17 August 2021
Available online 25 August 2021

KEYWORDS

BODIPY;
Fluorescent probe;
Tumor targeting;
Bioimaging;
Molecular docking

Abstract BODIPY derivatives have attracted much attention in the field of biological probes, but probes with a single imaging function are no longer innovative. In this paper, two multifunctional sulfonamide-BODIPY derivatives were designed and synthesized. Photophysical properties, cytotoxicity, *in vitro* and *in vivo* imaging, apoptosis, cell cycle, and molecular docking simulation were studied. The results showed that the compound had low cytotoxicity to normal cells, but had strong inhibitory effect on tumor cells. The IC_{50} value of compound **3** on HCT-116 cells was 58.61 ± 4.91 μmol/L, and **4** on HeLa cells was 52.29 ± 10.93 μmol/L. Cell imaging and mice experiments demonstrated that the probe had excellent biocompatibility and potential tumor targeting; and *in vivo* imaging of mice at different time periods showed that the fluorescence intensity of probes in subcutaneous lung tumor gradually increased with the extension of time. In addition, the flow cytometry analysis of **3** showed that the G1 phase of HCT-116 cells was inhibited and apoptosis of tumor cells was promoted. In molecular docking simulation, sulfonamide-BODIPY derivatives had high affinity scores with CDK2: −8.0 and −8.4 kcal·mol^{-1}, and the multiple interactions with receptors provided conditions for the probes to recognize tumor cells.

1. Introduction

In the past few decades, fluorescent probes have been a hot topic of chemists and biologists (Zhang et al., 2020; Qin et al., 2021; Long et al., 2019; Yang et al., 2019; Li et al., 2020). 4, 4-difluoro-4-bora-3a,4a-diaza-s-indacene (BODIPY) fluorescent dyes have attracted the attention of scholars for light stability, thermal stability and high molar absorption coefficient (Zhang et al., 2021; Li et al., 2021; Wang et al., 2021). To date, it has been developed as imaging probes, fluo-

* Corresponding author.
E-mail address: organicboron@ujs.edu.cn (G. Jin).
Peer review under responsibility of King Saud University.

Production and hosting by Elsevier

https://doi.org/10.1016/j.arabjc.2021.103395
1878-5352

rescent dyes, chemical sensors and photosensitizers (Qi et al., 2020; Dolati et al., 2020; Dagnaw et al., 2021; VanDenburgh et al., 2020; Khuong Mai et al., 2020; Tümay et al., 2016; Tang et al., 2020; Çetindere et al., 2016). However, as a bioprobe, BODIPY core has only a single labeling function, and has low hydrophilicity and no targeting (Kand et al., 2020; Kesavan et al., 2019). At present, only the single labeled probe has no longer novelty, and the multi-functional responsive target fluorescent probe can lead the future probe field.

The conventional method to improve the characteristics of compounds is to modify and optimize their structures directly (Thapaliya et al., 2020; Jin et al., 2020; Khan et al., 2021). In 2020, Rongkun modified BODIPY with formyl to detect biological biothiols in mitochondria and endoplasmic reticulum to improve the targeting of the probe (He et al., 2020). But this does not improve its hydrophilicity. Although many methods of modifying BODIPY with ionizable groups or combining with oxygen-rich groups have been reported, (Franke et al., 2019; Chen et al., 2020; Sui et al., 2016; Çetindere et al., 2019) these modifications still cannot comprehensively solve the problems of hydrophilicity, targeting and single functionality of BODIPY. After reviewing a large number of literatures, we turned our attention to the derivatives of sulfonamide.

Sulfonamide is a kind of inorganic small molecule, which is the raw material of many biomedicines, and has a wide range of applications in biology and pharmaceutical chemistry (Zimmermann et al., 2019; Bagul et al., 2017; Shao et al., 2018; Liu et al., 2019; Liu et al., 2019). Its derivatives have been reported to be antibacterial, anti-inflammatory, antitumor and anti-allergic effects (Apaydın and Török, 2019; Matsuura et al., 2021; Procopiou et al., 2017; Ali et al., 2019). In 2019, it was designed into different cyclobenzosulfonamide scaffolds, which can target tubulin as a new mitotic inhibitor (Zimmermann et al., 2019). Subsequently; 1,2,4-triazine sulfonamides were designed and synthesized, showing high antiproliferative activity against human breast cancer cell lines (Branowska et al., 2020). Sulfonamide-substituted BODIPYs have also been synthesized in the long-term research (Takeda et al., 2016; Waghorn et al., 2012). The introduction of sulfonamide group can enhance the following characteristics of probes: 1) water solubility; 2) biocompatibility; 3) drug activity; 4) targeting to tumor cells (Liu et al., 2019; Chan et al., 2019). BODIPY itself does not have any drug activity and targeting, but only has strong fluorescence effect. Therefore, the combination of BODIPY and sulfonamide can be designed into novel fluorescent drug-probes with both fluorescence effect, drug activity and a series of cytocompatibility and targeting effects.

Herein, we designed two kinds of multifunctional sulfonamide-BODIPY fluorescent probes, and analyzed their photophysical properties in different solvents; detected the cytotoxicity of the compounds; conducted *in vitro* and *in vivo* imaging; apoptosis; cell cycle experiment and molecular docking simulation. In order to better explore the ability of tumor targeting and imaging, we added *in vivo* imaging of subcutaneous lung tumor in mice at different time periods. In addition, a series of inhibitor activities were evaluated to explore the inhibitory effect of sulfonamide-BODIPY derivatives more comprehensively on tumor cells in targeted imaging. These investigations will be beneficial to the design and research of fluorescent probes for multifunctional targeting drugs in the future, which will be a significant breakthrough in BODIPY research field.

2. Experimental section

2.1. Reagents and instrumentation

All reagents were purchased commercially and further purified when used. All the reactions involved were monitored by thin-layer chromatography (TLC) and analyzed with ultraviolet lamps at 254 and 365 nm. Products were separated and purified by column chromatography (200–300 mesh silica gel). NMR were recorded by Bruker avance II instrument in deuterium chloroform (400 MHz for ^{1}H and 100 MHz for ^{13}C). Chemical shifts are reported in ppm, versus internal tetramethylsilane (TMS) as a standard. The mass spectrum were obtained on a Thermo LXQ by liquid chromatgraphy-ion trap mass spectrometry. Absorption spectra were recorded with a UV-2550 spectrophotometer. The fluorescence emission spectra were measured by Shimazu RF-5301PCS fluorescence spectrophotometer with excitation wavelength of 500 nm.

2.2. Synthesis

N1-(8-ethyl-5,5-difluoro-7,9-dimethyl-10-phenyl-5H-5λ^4,6λ^4-dipyrrolo[1,2-c:2′,1′-f][1,3,2] diaza -borinin-3-yl)ethane-1,2-diamine (2). 7-chloro-2-ethyl-5,5-difluoro-1,3-dimethyl-10-phenyl-5H-4λ^4,

5λ^4-dipyrrolo[1,2-c:2′,1′-f] (Zhang et al., 2020; Long et al., 2019; Qin et al., 2021) diazaborinine (**BODIPY-Cl**; 0.5 g, 1.4 mmol) was dissolved in acetonitrile (15 mL), ethylenediamine (300 μL, 4.5 mmol) and triethylamine (600 μL, 4.3 mmol) were added. The reaction was stopped after magnetic stirring at room temperature for 6 h. Red compound **2** (0.45 g, 85%) was isolated by column chromatography (petroleum ether: EtOAc = 1:1; dichloromethane: MeOH = 25:1). ^{1}H NMR (400 MHz, $CDCl_3$): δ (ppm) = 8.01 (s, 1H), 7.42–7.39 (m, 3H), 7.31–7.29 (m, 2H), 6.46 (d, J = 4.4 Hz, 1H), 5.92 (d, J = 4.8 Hz, 1H), 3.41 (s, 2H), 3.00 (t, J = 6.0 Hz, 2H), 2.47 (s, 3H), 2.35–2.29 (dd, J = 7.6, 14.8 Hz, 2H), 1.37 (s, 3H), 1.26 (s, 2H), 0.99 (t, J = 7.6 Hz, 3H). ^{13}C NMR (100 MHz, $CDCl_3$): δ (ppm) = 159.8, 144.9, 135.2, 133.3, 133.1, 132.4, 132.3, 130.0, 129.6, 128.3, 128.0, 106.0, 46.8, 41.4, 29.7, 17.1, 15.0, 11.9, 11.6. ITMS (ESI) calcd for $C_{21}H_{25}BF_2N_4$ $[M + H]^+$ m/z 383.2218; found 383.2345.

1-(2-((8-ethyl-5,5-difluoro-7,9-dimethyl-10-phenyl-5H-5λ^4,6λ^4-dipyrrolo[1,2-c:2′,1′-f][1,3,2]diazaborinin-3-yl)amino)ethyl) sulfonamide (4). **2** (0.1 g, 0.3 mmol) and sulfonamide (0.1 g, 1.0 mmol) were dissolved in 4 mL pyridine, heated to 80 °C under magnetic stirring for 2 h. After TLC confirmed that the reaction was complete, the reaction was stopped and cooled to room temperature. The pyridine solvent was dried under reduced pressure and column chromatography (petroleum ether: ethyl acetate = 2:1) was used to obtain brownish red compound 3 (42 mg, 35%). ^{1}H NMR (400 MHz, $CDCl_3$): δ (ppm) = 7.45–7.30 (m, 5H), 6.47 (d, J = 4.8 Hz, 1H), 6.34 (s, 1H), 6.94 (s, 1H), 5.29 (s, 1H), 5.07 (s, 2H), 3.53 (s, 2H), 3.40 (d, J = 4.4 Hz, 2H), 2.45 (s, 3H), 2.35–2.30 (dd,

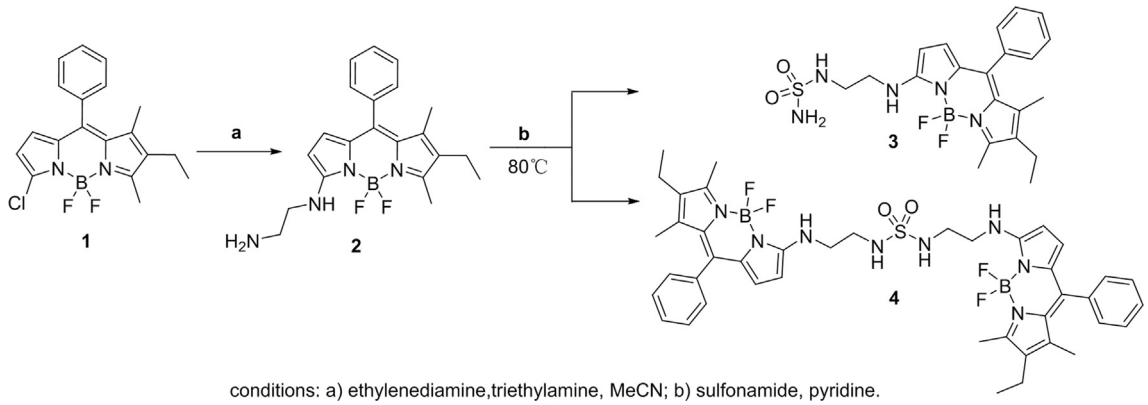

Scheme 1 Synthetic route of sulfonamide-BODIPY.

J = 14.8 Hz, 7.2 Hz, 2H), 1.39 (s, 3H), 1.00 (t, J = 7.6 Hz, 3H). ^{13}C NMR (100 MHz, $CDCl_3$): δ (ppm) = 159.5, 135.0, 133.8, 133.4, 133.0, 132.2, 130.4, 129.5, 128.5, 128.1, 118.5, 111.7, 105.8, 43.9, 43.2, 17.1, 14.9, 12.0, 11.6. ITMS (ESI) calcd for $C_{21}H_{26}BF_2N_5O_2S$ $[M + H]^+$ m/z 462.1948; found 462.2019.

1,3-bis(2-((8-ethyl-5,5-difluoro-7,9-dimethyl-10-phenyl-5H-5λ^4,6λ^4-dipyrrolo[1,2-c:2′,1′-f][1,3,2]diazaborinin-3-yl)amino) ethyl) sulfonamide (4). **2** (0.1 g, 0.3 mmol) and sulfonamide (0.03 g, 0.3 mmol) were dissolved in 4 mL pyridine and heated to 80 °C under magnetic stirring for 4 h. After TLC confirmed that the reaction was complete, the reaction was stopped and cooled to room temperature. The orange-red Compound **4** (20 mg, 10%) was isolated by column chromatography (petroleum ether: ethyl acetate = 5:1) after removing the pyridine solvent. ^{1}H NMR (400 MHz, $CDCl_3$): δ (ppm) = 7.45–7.31 (m, 8H), 8.44 (d, J = 4.4 Hz, 2H), 6.18 (s, 2H), 5.92 (d, J = 4.8 Hz, 2H), 5.01 (s, 2H), 3.49 (t, J = 5.6 Hz, 3H), 3.37 (t, J = 6.0 Hz, 3H), 2.48 (s, 4H), 2.36–2.30 (dd, J = 15.2 Hz, 7.6 Hz, 4H), 1.37 (d,

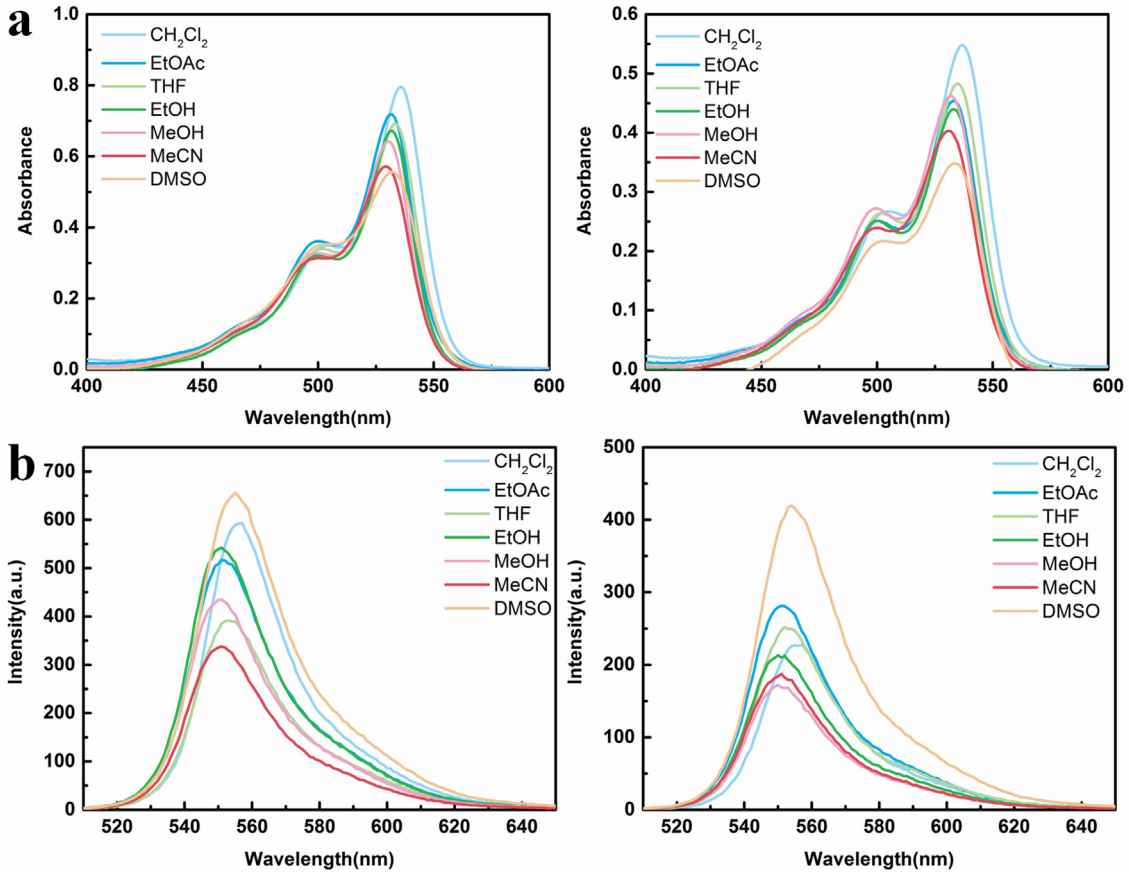

Fig. 1 (a) The absorption spectra of compounds **3** and **4** (c = 15 μmol/L) in different solvents are shown from left to right. (b) The emission spectra of **3** and **4** in different solvents (ex = 500 nm).

Table 1 Photophysical properties of compounds **3** and **4**.

Samples	Φ_f [a]	Wavelength	DCM	EtOAc	THF	EtOH	MeOH	MeCN	DMSO
3	0.33	Abs_{max} (nm)	536	531	533	531	530	530	531
		Em_{max} (nm)	555	551	552	551	550	551	555
		stokes shift (nm)	19	20	20	20	20	21	24
		stokes shift (cm^{-1})	639	683	646	684	686	719	850
4	0.25	Abs_{max} (nm)	536	533	534	533	531	531	533
		Em_{max} (nm)	555	551	552	550	550	550	555
		stokes shift (nm)	19	18	18	17	19	19	22
		stokes shift (cm^{-1})	639	613	545	580	650	650	744

[a] Fluorescence quantum yield of the compounds in DMSO estimated relative to rhodamine B as the standard (Φ_f = 0.7 in ethanol).

J = 10.4 Hz, 6H), 1.29 (d, *J* = 11.6 Hz, 6H), 1.00 (t, *J* = 7.6 Hz, 6H). ^{13}C NMR (100 MHz, $CDCl_3$): δ (ppm) = 159.6, 147.8, 147.7, 147.1, 145.5, 145.4, 135.0, 133.0, 130.4, 129.6, 128.5, 128.1, 124.5, 124.0, 119.1, 105.8, 43.9, 43.1, 34.9, 34.5, 31.4, 30.2, 29.7, 22.7, 17.1, 14.9, 12.0, 11.6. ITMS (ESI) calcd for $C_{42}H_{48}B_2F_4N_8O_2S$ $[M + H]^+$ *m*/*z* 827.3823; found 827.1713.

2.3. Cytotoxicity determination

HCT-116, HeLa and normal liver L-02 cells from American type culture collection were used for cytotoxicity screening *in vitro*. HCT-116 and HeLa cells were routinely cultured in RPMI-1640 medium, while L-02 cells were cultured in DMEM medium routinely. 10% fetal bovine serum (FBS) was added to the medium, and the cells were incubated in a 5% CO_2 cell incubator at 37 °C. Monitor these cells daily and keep the cell density at 80%.

MTT cancer cells (HeLa and HCT-116) and normal human lung L-02 were used to determine the cytotoxicity of each cell line during logarithmic growth phase, respectively. All cells were inoculated on 96-well plate at the rate of 106 cells / well. Then the samples were treated with 1, 2, 6, 8 or 10 mmol/mL berberine and detected for 24 h. The supernatant was dissolved in 100 mL DMSO and shaken for 15 min. The optical density of the sample was measured at 490 nm by microplate photometer. Cell viability was expressed as a percentage change in absorbance relative to the control value.

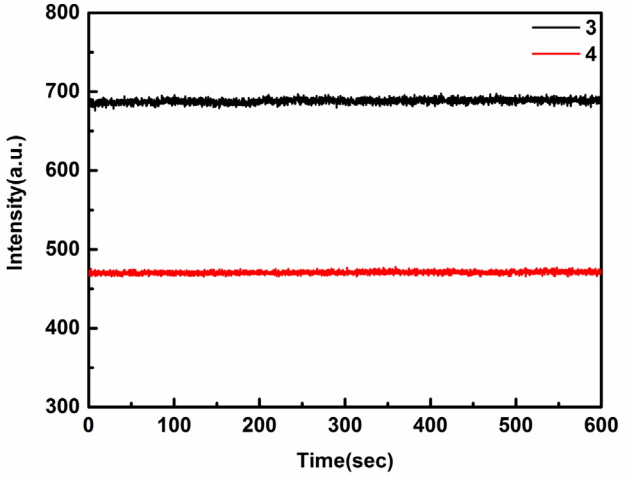

Fig. 3 Fluorescence stability of **3** and **4** (15 μmol/L) in DMSO solution (Ex = 430 nm, Em = 555 nm).

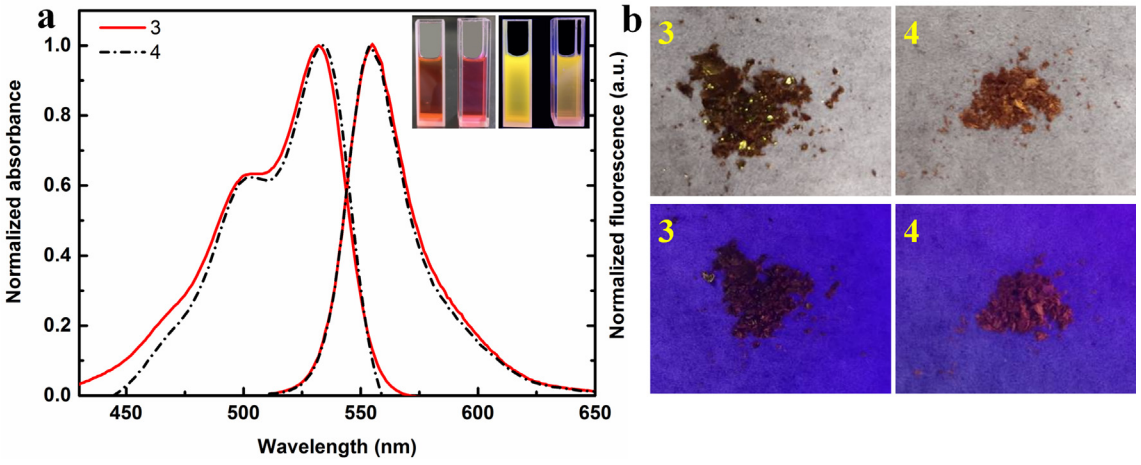

Fig. 2 (a) Normalized UV–Vis and Fluorescence spectra of compounds **3** and **4** (C = 15 μmol/L) in DMSO solution. The illustration is a comparison of **3** and **4** in DMSO solution under sunlight and ultraviolet light. (b) Sunlight and fluorescence images of **3** and **4** solid powders at 365 nm excitation wavelength.

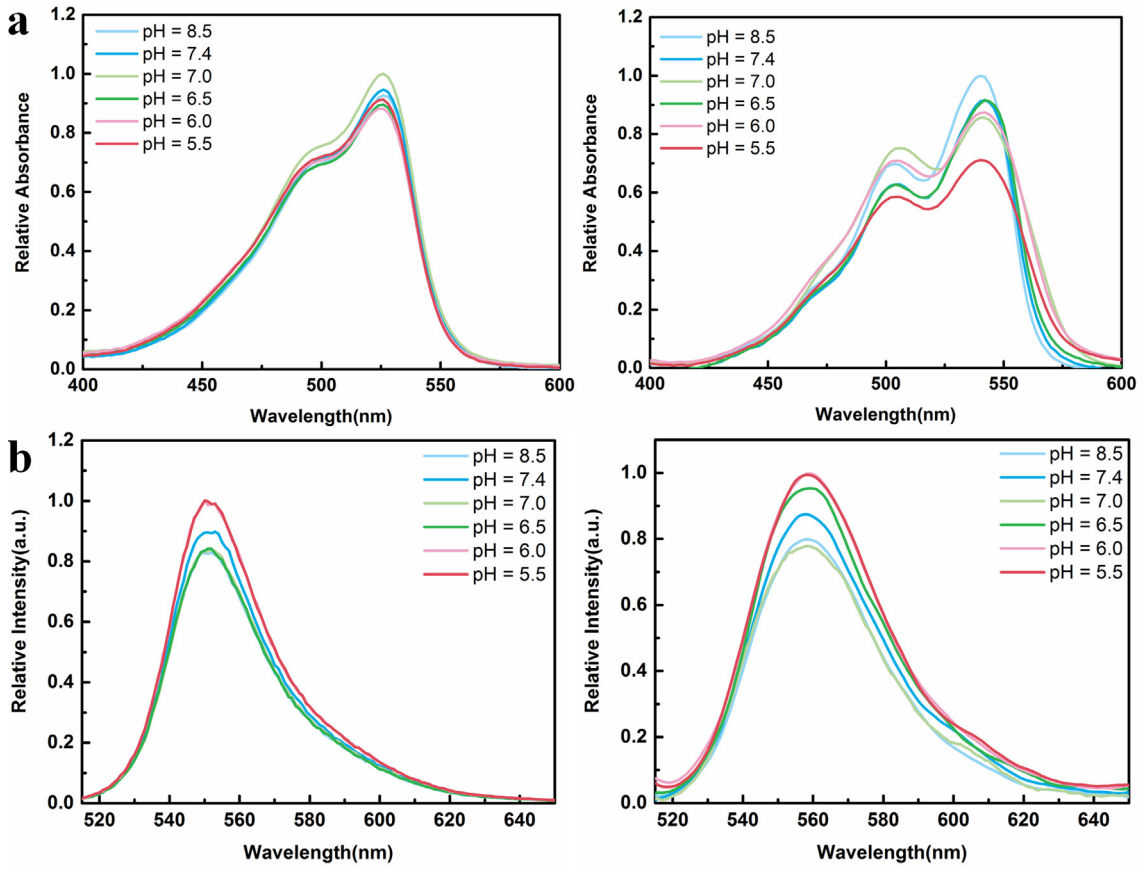

Fig. 4 (a) The absorption spectra of **3** and **4** (C = 15 μmol/L) at different pH values are shown from left to right. (b) Emissivity spectra of **3** and **4** at different pH (ex = 500 nm).

2.4. Cell imaging

HeLa cells in logarithmic growth phase were digested with trypsin and inoculated into 9-well-plate with round cap. They were cultured in 5% CO_2 and 37 °C incubator for 24 h before adhering. Drug treatment: Compounds **3** and **4** were weighed and added into DMSO (C = 0.10 mmol/L), respectively, and diluted to 10 μmol/L. Drug adding process: the original medium was discarded and replaced with the medium containing 10 μmol/L different drugs. Cell treatment: discard the medium after 24 h, wash it with PBS for 3 times, add paraformaldehyde fixed solution for 15 min, and carefully suction out. Wash with PBS for 3 times and incubate it with 4′,6-diamidino-2-phenylindole dye (DAPI) in dark for 10 min. Discard the staining solution and wash it with PBS for 3 times. After sealing with anti-fluorescence quenching sealant, the changes of the sample and nucleus were observed under fluorescence microscope.

2.5. In vivo imaging

In vivo imaging experiments were performed on mice weighing 18.3 g and 18.5 g at 6 weeks of age. After compounds **3** and **4** (20 μL, 20 μmol/L dimethylsulfoxide/normal saline = 1:9, V/V) were injected into an empty stomach for 30 min, the fluorescence intensity of subcutaneous tumor tissues was detected. In addition, the mice experiment met the requirements of Animal Ethics (ethics committee approval No. syxk 2018–0053).

Mice imaging at different time periods: Compounds **3** and **4** were prepared (20 μmol/L, 20 μL DMSO/normal saline = 1:9, V/V) and intraperitoneally injected into 8-week-old mice, respectively, all weighing 21.8 g. Fluorescence intensity of subcutaneous lung tumor was detected every 10 min (10 min, 20 min, 30 min and 40 min).

2.6. Cell cycle experiments

HCT-116 cells were cultured in a 9-well culture plate and then treated with compound **3**. Cell suspensions were cultured at 37 °C with trypsin and then placed in pre-cooled 75% ethanol at –23 °C overnight. The ribozyme (25 μg/mL) and propidium iodide (25 μg/mL PI; BD Biosciences (Anolun Biotechnology Co., Ltd, Beijing)) was added to the cells and cultured in room temperature darkness for 30 min. The samples were then evaluated using flow cytometry (Attune NXT, Life Tech, LNC), and the data were analyzed using Modfit LT2.0 software (Verity Software House, Inc., Topsham, ME, USA).

2.7. Cell apoptosis

HCT-116 cells were cultured in a 9-well culture plate. Cells were treated with compound **3**. The cell suspension was col-

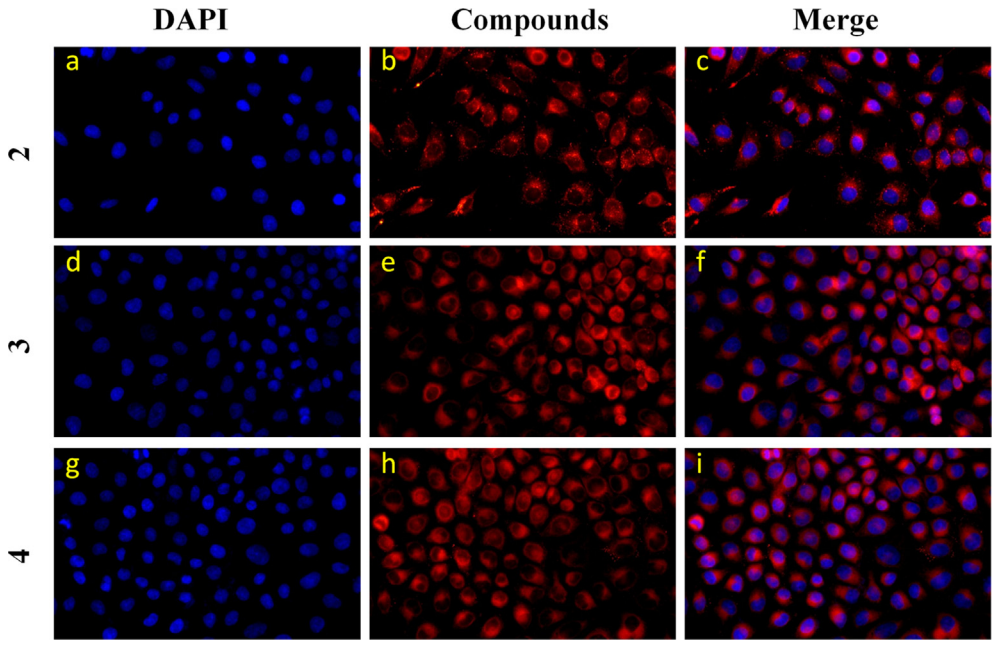

Fig. 5 Confocal microscope images of HeLa cells incubated with compounds 2, 3 and 4 (10 μmol/L) for 24 h. The nuclei were stained with DAPI. Compound 2: 200 units high density; Compounds 3 and 4: 400 units low density.

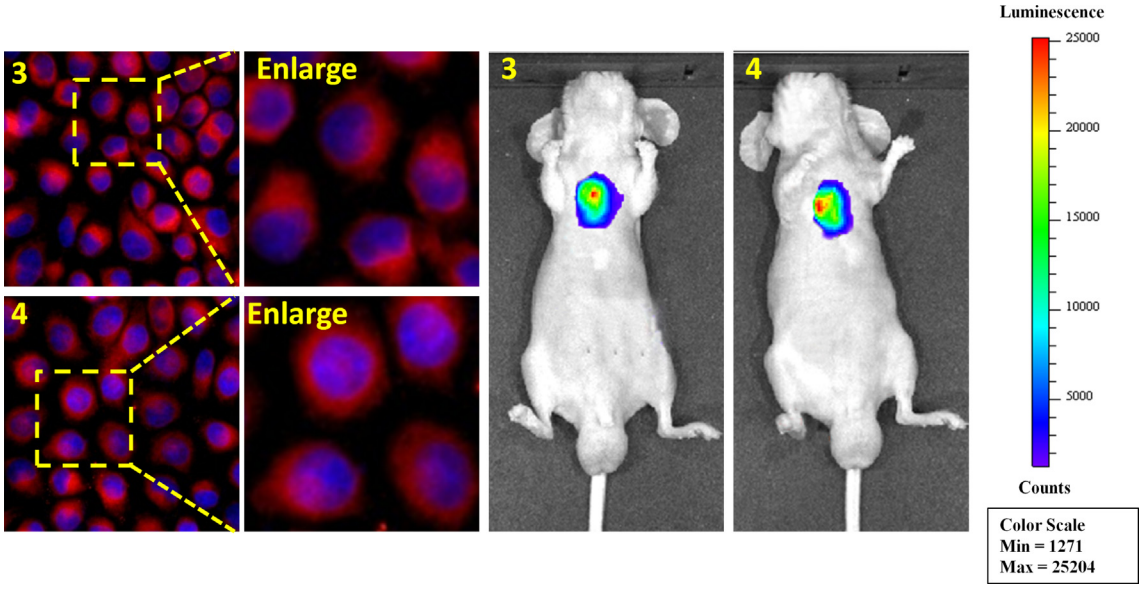

Fig. 6 Merged images in HeLa cells of **3** and **4** (left) and subcutaneous tumor tissue in mice (right).

lected by trypsin at 37 °C without EDTA, washed with PBS, and resuspended with 250 mL binding buffer. The cell suspension was stained with 5 μL PI and 5 μL fluorescein isothiocyanate of annexin V solution (Yasen Biotechnology, Shanghai, Co., Ltd) and incubated at room temperature in darkness for 20 min. The samples were then evaluated by flow cytometry (Attune NXT, LifeTech, LNC). All test methods are in triplicate.

3. Results and discussion

3.1. Design and synthesis

Using 7-chloro-2-ethyl-5,5-difluoro-1,3-dimethyl-10-phenyl-5 H-4λ^4,5λ^4-dipyrrolo[1,2-c:2′,1′-f] [1,3,2] diazaborinine as a chemical material (Zhao et al., 2013); and triethylamine as the deacid reagent in acetonitrile solvent; compound **2**

(yield = 85%) was obtained by nucleophilic substitution of **1** and ethylenediamine. Figure Scheme 1 Dissolve **2** in pyridine solvent, and add different equivalent sulfonamide to get two sulfonamide-BODIPY derivatives at 80 °C. The synthesis method was simple, and the chemical structures of the products were confirmed by ^{1}H NMR, ^{13}C NMR and ITMS. (See supporting information for characterization data).

3.2. Spectroscopic properties

Compounds **3** and **4** (C = 15 μmol/L) were prepared with dichloromethane, ethyl acetate, tetrahydrofuran, ethanol, methanol, acetonitrile and dimethyl sulfoxide as solvents, respectively. The absorbance at 400–600 nm and fluorescence intensity at 510–650 nm were measured (Fig. 1). It is easy to observe that the absorbance decreases with the increase of solvent polarity. The difference is that under the excitation of 500 nm, the fluorescence intensity of the two compounds is the strongest in DMSO. It is speculated that the amino group in the probe is likely to form intermolecular hydrogen bonds with DMSO. At this time, the energy of the system is reduced, and the molecular stability is increased, so the UV absorbance is low. However, DMSO has a strong stabilizing effect on excited fluorescent molecules and reduces the internal conversion rate between excited molecules, so the fluorescence in polar solvent DMSO is strong. (Wang et al., 2021; Zakerhamidi et al., 2011)

The photophysical data of the compounds in different solvents are summarized in Table 1 (maximum wavelength absorption: Absmax, maximum emission: Emmax) and Fig. 2. In different solvents, the maximum emission wavelength of **3** and **4** fluctuates in the range of 550–555 nm. Compounds **3**, **4** both have the largest stokes shift in DMSO solvent, and the maximum emission wavelengths of compounds have a small red shift compared with other solvents. Because of the hydrogen bonds among the compounds and DMSO solvent, the energy level difference between the excited state and the ground state decreases, the emission spectrum of the probes is red shifted.

According to UV–Vis fluorescence comparison of compounds in DMSO solution (Fig. 2), it can be found that stokes shift of **3** and **4** is 850 and 744 cm^{-1}, respectively. Due to steric hindrance, it is more difficult for compound **4** to form hydrogen bond force with DMSO than compound **3**, so the stokes shift of compound **4** is less than **3**. The illustration shows the compound solution is red, **3** and **4** are yellow and orange fluorescence respectively. The solid powder is shown in Fig. 2b. Under the excitation wavelength of 365 nm, the fluorescence of powder **3** is not obvious, while that of powder **4** shows red. In addition, the fluorescence stability of sulfamide-substituted-BODIPY at 10 min was recorded (Fig. 3). Obviously, these two compounds remain dynamically stable over time in DMSO solvent.

In 10% (volume fraction) DMSO / Tris-HCl buffer solution, dilute hydrochloric acid was added and adjusted to pH = 8.5, 7.4, 7.0, 6.5, 6.0, 5.5, respectively. The absorption and emission spectra of compounds **3** and **4** at different pH were recorded (Fig. 4). The absorbance of the two compounds decreased relatively under weak acid condition, but the fluorescence intensity was stronger at pH = 6.0 and 5.5. It is speculated that under weak acidic conditions, the compound may be easily protonated, which prevents the intramolecular charge transfer from nitrogen in BODIPY, so the emission intensity is enhanced. Under the influence of polar solvent, the probe forms intermolecular hydrogen bond with the solvent, which affects the absorbance. (Prasannan et al., 2018) Generally speaking, the tumor cells are weakly acidic. In this environment, the fluorescence of compounds can be enhanced to a greater extent, which is conducive to the labeling of tumor cells.

Table 2 Experimental data of cytotoxicity.

Compounds	IC_{50} (μmol/L) ± SD[a]		
	HCT-116	HeLa	L-02
3	58.61 ± 4.91	61.08 ± 8.11	113.41 ± 8.34
4	79.43 ± 8.20	52.29 ± 10.93	104.89 ± 12.07
5-FU	24.17 ± 3.83	18.53 ± 2.06	> 200

[a] Standard deviation.

3.3. Cytotoxicity studies

Compounds **3** and **4** were used to determine the cell activity of HCT-116, HeLa and human normal liver cells L-02, (Khalil et al., 2020; Eldehna et al., 2018) respectively (Table 2). With 5-FU as control, IC_{50} > 200 μmol/L indicates that the 5-FU has low toxicity to L-02 cells. It was obvious that compounds **3** and **4** have low cytotoxicity to normal hepatocytes, but have significant inhibitory effects on HCT-116 and HeLa cells. Among them, **3** has more obvious inhibitory effects on HCT-116 and **4** on HeLa cells, with IC_{50} values of 58.61 ± 4.91 and 52.29 ± 10.93 μmol/L respectively.

3.4. In vivo and in vivo imaging

In Fig. 5, *in vitro* imaging of sulfamide-substituted-BODIPY probes were further studied. Obviously, compounds **2**, **3** and **4** can be fully absorbed by HeLa cells. (Wang et al., 2021) In addition, the introduction of sulfonamide group into intermediate compound **2** will not affect the absorption of probes by HeLa cells. All shows the good biocompatibility of sulfamide-substituted-BODIPY.

To further enhance subsequent biological research, we performed the most basic imaging study on mice. **3** and **4** were intraperitoneally injected into the tumors tissue of mice, respectively, and fluorescence imaging was performed 30 min later. As shown in Fig. 6, strong fluorescence signals were detected in the subcutaneous lung tumor tissues of both mice, indicating that the sulfamide-substituted-BODIPY probes have the ability to monitor tumor tissues. On this basis, we carried out imaging experiments on mice at different times (Fig. 7). With the prolongation of time, compounds **3** and **4** gradually aggregated to the tumor site of mice, and the fluorescence intensity gradually increased. This further demonstrates the excellent tumor targeting ability of sulfamide-substituted-BODIPY probes.

3.5. Apoptosis and cell cycle

The apoptosis and cell cycle of HCT-116 cells treated with compound **3** which was randomly selected were studied. In

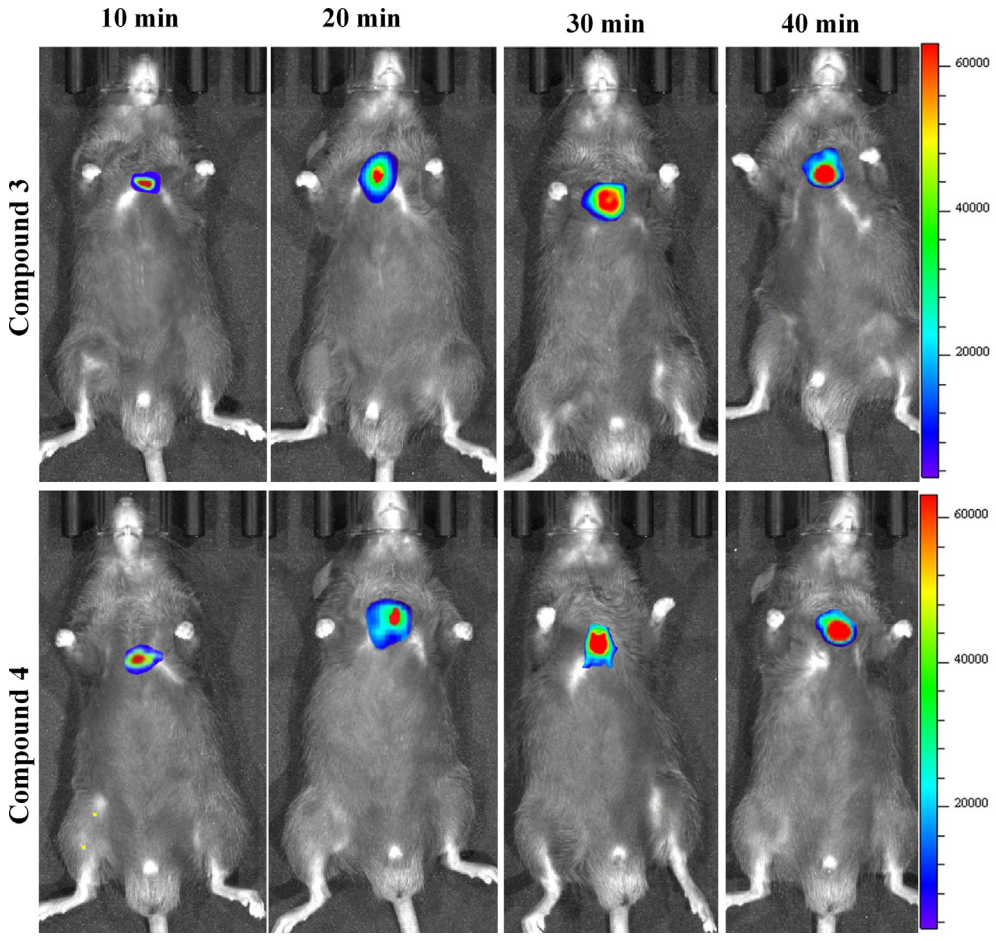

Fig. 7 Fluorescence imaging of subcutaneous lung tumor tissue of mice with compounds **3** and **4** (20 μmol/L) at different time intervals (10 min, 20 min, 30 min and 40 min).

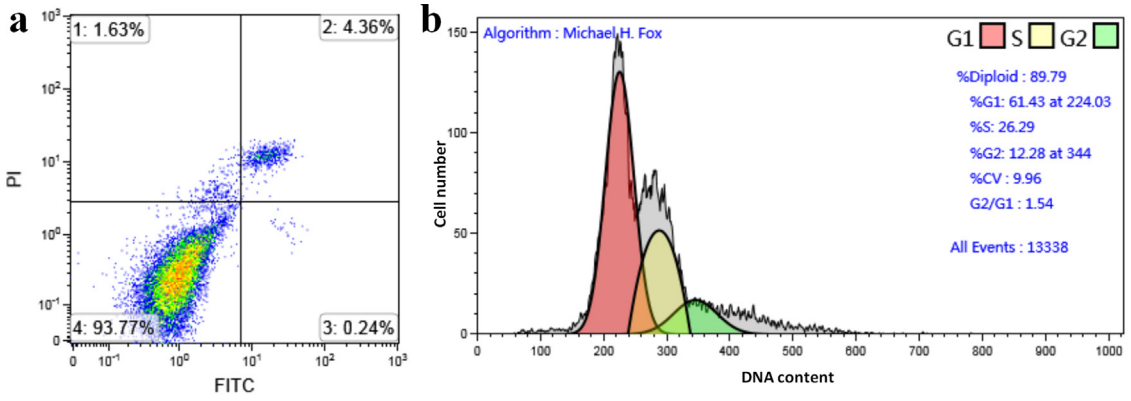

Fig. 8 (a) HCT-116 cells were treated with **3** and stained with PI and Annexin-V /FITC; then analyzed for apoptosis. (b) HCT-116 cells were treated with compound **3** and the cell cycle was analyzed by flow cytometry.

Fig. 8a, The lower right quadrant is the early apoptotic cells (Ashokkumar et al., 2019; Sun et al., 2021; Zhou et al., 2020; Wu et al., 2019; Yang et al., 2019). After treatment with **3**, the percentage of living cells was 93.77%. The early apoptotic cell rate and late apoptotic cell rate were 0.24%, 4.36% respectively, and the total apoptotic rate was 4.6%. Fig. 8b showed that the average DNA content of G1 phase was 224.03, and the number of G1 phase cells accounted for 61.43% of the total. In addition, G2 / G1 = 1.54, which indicated that the number of cells in G1 phase of HCT-116 increased, so compound **3** could block the G1 phase of HCT-116 cells. The above data well demonstrated that compound **3** had a good

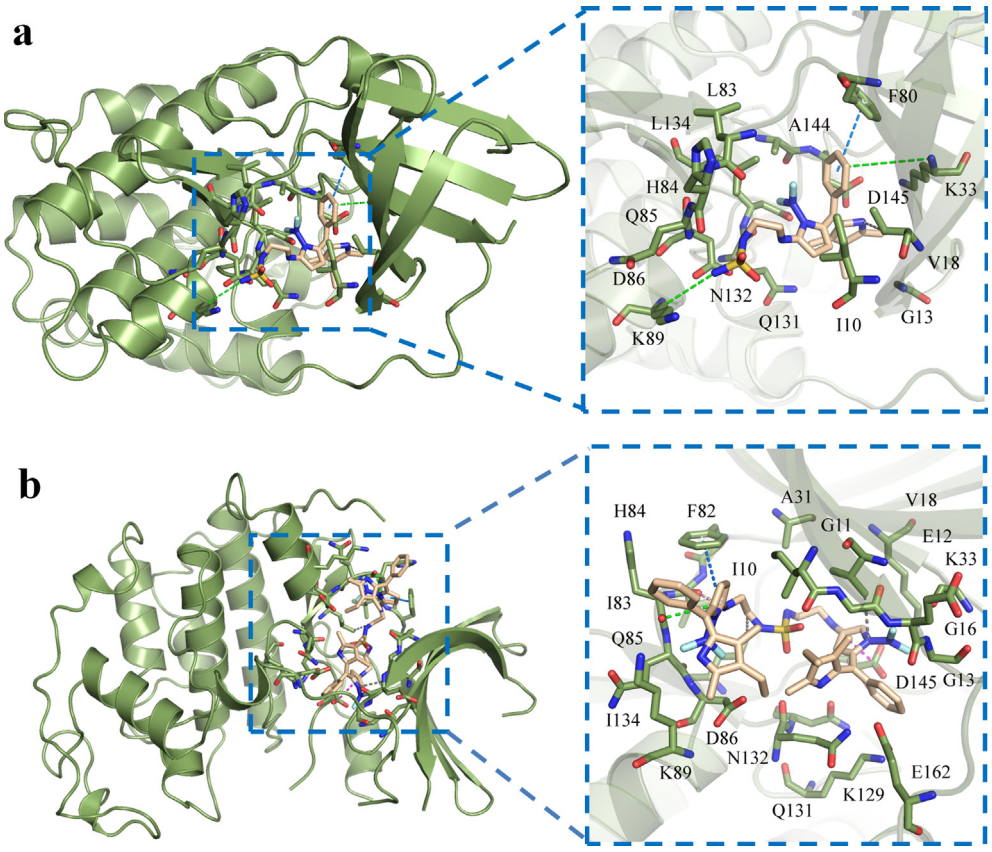

Fig. 9 Molecular docking diagram of sulfamide-substituted-BODIPY and CDK2. (a) Compound **3**; (b) compound **4**. (different interactions are represented by dotted lines of different colors – ion π: green; T-π: marine; hydrogen bond: pin; hydrophobic bond: gray; ionic bridge: magenta).

Table 3 Interaction between residues and compounds (PDBID: 2FVD).

Entry	Affinity score	Interaction with receptor				
(PDBID 2FVD)	(kcal·mol^{-1})	[H]	T-π	Ion-π	Hydrophobic bond	ionic bridge
3	-8.0	His 84 Gln 131	Phe 80	Asp 86 Asp 145 Lys 33 Lys 89 His 84	Ala 144 Ile 10 Leu 83 Leu 134 Phe 80 Val 18	Asp 86
4	-8.4	Leu 83	Phe 82	Asp 86 Asp 145 Lys 33 Glu 12 Glu 162 His 84	Ala 31 Leu 83 Leu 134 Phe 82 Val 18	Asp 145

inhibitory effect on HCT-116 cells, and showed that sulfamide-substituted-BODIPY had the potential of inhibiting tumor cell activity as a probe at the same time.

3.6. Molecular docking

In order to elucidate the mechanism of action of the compound on tumor cells as much as possible, molecular docking simulation was performed on the tumor cell target CDK2 kinase (Chen et al., 2016; Shao et al., 2021; Alnoman et al., 2020; Shi et al., 2020), and its corresponding affinity score was obtained (Fig. 9 and Table 3). Compounds **3**,**4** and receptor had high binding energies of −8.0 and −8.4 kcal•mol-1, respectively. There are hydrogen bond, T-π, Ion-π, Hydrophobic bond and ionic bridge interactions between these probes and receptors. In compound 3, the oxygen atoms on sulfon-

amide form hydrogen bonds with the hydrogen atoms of His 84; the benzene ring on BODIPY forms T-π stacking with Phe 80; the amino group on sulfonamide forms ionic bridge with Asp 86. In compound **4**, the nitrogen atom on sulfonamide has hydrogen bonding with the hydrogen atom on Leu 83. The pyrrole ring directly linked to ethylenediamine can form a T-π stacking with Phe 82. These interactions between the compounds and the receptors provide the conditions for the new sulfamide-substituted-BODIPY s to recognize tumor cells.

4. Conclusion

In conclusion, two multifunctional sulfonamide-BODIPY fluorescent probes were successfully synthesized. Its advantages include hydrophilicity, high biocompatibility, inhibition of tumor cell proliferation and potential targeting imaging. Oxygen-rich sulfonamides can increase the hydrophilic ability of probes, and use its unique drug activity to achieve inhibition of tumor cells. In weak acid environment, it shows fluorescence enhancement, which is beneficial to the imaging of tumor cells with weak acid pH. Cell imaging and mice imaging show that these probes have good biocompatibility and potential targeting properties. The novel sulfamide-substituted-BODIPY drug probe has potential applications in tumor cell targeting and exerting drug activity; the introduction of the concept can also provide a strong basis for the design of drug probes with high selectivity, high activity, high biocompatibility and excellent tumor targeting.

Declaration of Competing Interest

The authors declare that they have no known competing financial interests or personal relationships that could have appeared to influence the work reported in this paper.

Acknowledgements

We would like to thank the scientific research foundation of Jiangsu University (Grant No. 5501290005). for the financial supports.

Appendix A. Supplementary data

Supplementary data to this article can be found online at https://doi.org/10.1016/j.arabjc.2021.103395.

References

Zhang, J., Wang, N., Ji, X., Tao, Y., Wang, J., Zhao, W., 2020. BODIPY-based fluorescent probes for biothiols. Chem - Eur J. 26 (19), 4172–4192. https://doi.org/10.1002/chem.v26.1910.1002/chem.201904470.

Qin, T., Liu, B., Xu, Z., Yao, G., Xu, H., Zhao, C., 2021. Flavonol-based small-molecule fluorescent probes. Sens Actuators, B. 336, 129718. https://doi.org/10.1016/j.snb.2021.129718.

Long, L., Cao, S., Jin, B., Yuan, X., Han, Y., Wang, K., 2019. Construction of a novel fluorescent probe for on-site measuring hydrogen sulfide levels in food samples. Food Anal Method. 12 (4), 852–858.

Yang, R., Mu, W.Y., Chen, Q.Y., 2019. Urazole-au nanocluster as a novel fluorescence probe for curcumin determination and mitochondria imaging. Food Anal Method. 12, 1805–1812 https://doi:10.1007/s12161-019-01519-2.

Li, W., Hu, X., Li, Q., Shi, Y., Zhai, X., Xu, Y., Li, Z., Huang, X., Wang, X., Shi, J., Zou, X., Kang, S., 2020. Copper nanoclusters @ nitrogen-doped carbon quantum dots-based ratiometric fluorescence probe for lead (II) ions detection in porphyra. Food Chem. 320, 126623. https://doi.org/10.1016/j.foodchem.2020.126623.

Zhang, H., Wang, L., Dong, P., Mao, S., Mao, P.u., Liu, G., 2021. Photolysis of the BODIPY dye activated by pillar[5]arene. RSC Adv. 11 (13), 7454–7458.

Li, H., Lv, F., Guo, X., Wu, Q., Wu, H., Tang, B., Yu, C., Wang, H., Jiao, L., Hao, E., 2021. Direct C-H alkoxylation of BODIPY dyes via cation radical accelerated oxidative nucleophilic hydrogen substitution: a new route to building blocks for functionalized BODIPYs. Chem Commun. 57 (13), 1647–1650.

Wang, S., Wang, Z., Gao, H.u., Jiang, L., Liu, H., Wu, F., Zhao, Y., Chan, K.S., Shen, Z., 2021. Highly regioselective palladium-catalyzed domino reaction for post-functionalization of BODIPY. Chem Commun. 57 (14), 1758–1761.

Qi, S., Kwon, N., Yim, Y., Nguyen, V.-N., Yoon, J., 2020. Fine-tuning the electronic structure of heavy-atom-free BODIPY photosensitizers for fluorescence imaging and mitochondria-targeted photodynamic therapy. Chem Sci. 11 (25), 6479–6484.

Dolati, H., Haufe, L.C., Denker, L., Lorbach, A., Grotjahn, R., Hörner, G., Frank, R., 2020. Two π-electrons make the difference: From BODIPY to BODIIM switchable fluorescent dyes. Chem - Eur J. 26 (6), 1422–1428. https://doi.org/10.1002/chem.v26.610.1002/chem.201905344.

Dagnaw, F.W., Cai, Y.-P., Song, Q.-H., 2021. Rapid and sensitive detection of nerve agent mimics by meso-substituted BODIPY piperazines as fluorescent chemosensors. Dyes Pigm. 189, 109257. https://doi.org/10.1016/j.dyepig.2021.109257.

VanDenburgh, K.L., Liu, Y., Sadhukhan, T., Benson, C.R., Cox, N. M., Erbas-Cakmak, S., Qiao, B.o., Gao, X., Pink, M., Raghavachari, K., Flood, A.H., 2020. Multi-state amine sensing by electron transfers in a BODIPY probe. Org Biomol Chem. 18 (3), 431–440.

Khuong Mai, D., Kang, B., Pegarro Vales, T., Badon, I.W., Cho, S., Lee, J., Kim, E., Kim, H.-J., 2020. Synthesis and photophysical properties of tumor-targeted water-soluble BODIPY photosensitizers for photodynamic therapy. Molecules. 25 (15), 3340. https://doi.org/10.3390/molecules25153340.

Tümay, S.O., Okutan, E., Sengul, I.F., Özcan, E., Kandemir, H., Doruk, T., Çetin, M., Çoşut, B., 2016. Naked-eye fluorescent sensor for Cu(II) based on indole conjugate BODIPY dye. Polyhedron. 117, 161–171 https://doi:10.1016/j.poly.2016.05.056.

Tang, F.K., Zhu, J., Kong, F.K.W., Ng, M., Bian, Q., Yam, V.-W.-W., Tse, A.K.W., Tse, Y.C., Leung, K.C.F., 2020. A BODIPY-based fluorescent sensor for the detection of Pt^{2+} and Pt drugs. Chem Commun. 56, 2695–2698 https://doi:10.1039/d0cc00027b.

Çetindere, S., Tümay, S.O., Kılıç, A., Durmuş, M., Yeşilot, S., 2016. Hexa-BODIPY linked-triazole based on a cyclotriphosphazene core as a highly selective and sensitive fluorescent sensor for fe2 + ions. J Fluoresc. 26, 1173–1181 https://doi:10.1007/s10895-016-1797-0.

Kand, D., Liu, P., Navarro, M.X., Fischer, L.J., Rousso-Noori, L., Friedmann-Morvinski, D., Winter, A.H., Miller, E.W., Weinstain, R., 2020. Water-soluble BODIPY photocages with tunable cellular localization. J Am Chem Soc. 142 (11), 4970–4974.

Kesavan, P.E., Pandey, V., Raza, M.K., Mori, S., Gupta, I., 2019. Water soluble thioglycosylated BODIPYs for mitochondria targeted cytotoxicity. Bioorg Chem. 91, 103139. https://doi.org/10.1016/j.bioorg.2019.103139.

Thapaliya, E.R., Mazza, M.M.A., Cusido, J., Baker, J.D., Raymo, F. M., 2020. A Synthetic strategy for the structural modification of photoactivatable BODIPY-oxazine dyads. Chem Photo Chem. 4 (5), 332–337. https://doi.org/10.1002/cptc.v4.510.1002/cptc.201900276.

Jin, G., Xiao, F., Li, Z., Qi, X., Zhao, L., Sun, X., 2020. Design, synthesis, and dual evaluation of quinoline and quinolinium iodide salt derivatives as potential anticancer and antibacterial agents. Chem Med Chem. 15 (7), 600–609. https://doi.org/10.1002/cmdc.v15.710.1002/cmdc.202000002.

Khan, H., Belwal, T., Efferth, T., Farooqi, A.A., Sanches-Silva, A., Vacca, R.A., Nabavi, S.F., Khan, F., Prasad Devkota, H., Barreca, D., Sureda, A., Tejada, S., Dacrema, M., Daglia, M., Suntar, İ., Xu, S., Ullah, H., Battino, M., Giampieri, F., Nabavi, S.M., 2021. Targeting epigenetics in cancer: therapeutic potential of flavonoids. Crit Rev Food Sci Nutr. 61 (10), 1616–1639.

He, R., Zhang, Y., Madhu, S., Gao, Q., Lian, Q., Raghavan, S.S., Geng, J., 2020. BODIPY based realtime, reversible and targeted fluorescent probes for biothiol imaging in living cells. Chem Commun. 56 (93), 14717–14720.

Franke, J.M., Raliski, B.K., Boggess, S.C., Natesan, D.V., Koretsky, E.T., Zhang, P., Kulkarni, R.U., Deal, P.E., Miller, E.W., 2019. BODIPY fluorophores for membrane potential imaging. J Am Chem Soc. 141 (32), 12824–12831.

Chen, N., Kommidi, H., Guo, H., Yang, X., 2020. lysosome specific, acidic-pH activated, near-infrared Bodipy fluorescent probe for noninvasive, long-term, *in vivo* tumor imaging. Mater Sci Eng C. 111,. https://doi.org/10.1016/j.msec.2020.110762 110762.

Sui, B., Tang, S., Woodward, A.W., Kim, B., Belfield, K.D., 2016. A BODIPY-Based water-soluble fluorescent probe for mitochondria targeting. Eur J Org Chem. 2016 (16), 2851–2857. https://doi.org/10.1002/ejoc.v2016.1610.1002/ejoc.201600238.

Çetindere, S., Okutan, E., Tümay, S.O., Yeşilot, S., Kılıç, A., 2019. Novel water-soluble cyclotriphosphazene-BODIPY conjugates: Synthesis, characterization and photophysical properties. J Fluoresc. 29, 1143–1152 https://doi:10.1007/s10895-019-02424-x.

Zimmermann, S., Akbarzadeh, M., Otte, F., Strohmann, C., Sankar, M.G., Ziegler, S., Pahl, A., Sievers, S., Kumar, K., 2019. A scaffold-diversity synthesis of biologically intriguing cyclic sulfonamides. Chem - A Eur J. 25 (68), 15498–15503. https://doi.org/10.1002/chem.v25.6810.1002/chem.201904175.

Bagul, S.D., Rajput, J.D., Tadavi, S.K., Bendre, R.S., 2017. Design, synthesis and biological activities of novel 5-isopropyl-2-methylphenolhydrazide-based sulfonamide derivatives. Res Chem Intermed. 43, 2241–2252 https://doi:10.1007/s11164-016-2759-5.

Shao, Z., Liu, W., Tao, H., Liu, F., Zeng, R., Champagne, P.A., Cao, Y., Houk, K.N., Liang, Y., 2018. Bioorthogonal release of sulfonamides and mutually orthogonal liberation of two drugs. Chem Commun. 54 (100), 14089–14092.

Liu, W., Deng, W., Sun, S., Dietrich, J.A., 2019. Strategy for the synthesis of sulfonamides on DNA. Org Lett 21, 9909–9913 https://doi:10.1021/acs.orglett.9b03843.

Liu, P., Lu, Z., Liu, L., Li, R., Liang, Z., Shen, M., Xu, H., Ren, D., Ji, M., Yuan, S., Shang, D., Zhang, Y., Liu, H., Tu, Z., 2019. NOD-like receptor signaling in inflammation-associated cancers: From functions to targeted therapies. Phytomedicine. 64, 152925. https://doi.org/10.1016/j.phymed.2019.152925.

Apaydın, S., Török, M., 2019. Sulfonamide derivatives as multi-target agents for complex diseases. Bioorg Med Chem Lett. 29 (16), 2042–2050. https://doi.org/10.1016/j.bmcl.2019.06.041.

Matsuura, R., Kanehara, R., Kadoya, A., Suzuki, S., 2021. Adsorption of sulfonamides to marine diatoms and arthropods. Environ Toxicol Pharmacol. 82, 103557. https://doi.org/10.1016/j.etap.2020.103557.

Procopiou, P.A., Ford, A.J., Gore, P.M., Hancock, A.P., Hodgson, S. T., Holmes, D.S., Looker, B.E., Vile, S., Clark, K.L., Saunders, K. A., Slack, R.J., Watts, C.J., 2017. Identification of selective 8-(piperidin-4-yloxy)quinoline sulfone and sulfonamide histamine H1 receptor antagonists for use in allergic rhinitis. Bioorg Med Chem Lett. 27 (21), 4914–4919. https://doi.org/10.1016/j.bmcl.2017.09.020.

Ali, S.S., Kenawy, E.-R., Sonbol, F.I., Sun, J., Al-Etewy, M., Ali, A., Huizi, L., El-Zawawy, N.A., 2019. Pharmaceutical potential of a novel chitosan derivative schiff base with special reference to antibacterial, anti-biofilm, antioxidant, anti-inflammatory, hemocompatibility and cytotoxic activities. Pharm Res. 36 (1). https://doi.org/10.1007/s11095-018-2535-x.

Branowska, D., Karczmarzyk, Z., Wolińska, E., Wysocki, W., Morawiak, M., Urbańczyk-Lipkowska, Z., Bielawska, A., Bielawski, K., 2020. 1,2,4-triazine sulfonamides: Synthesis by sulfenamide intermediates, *in vitro* anticancer screening, structural characterization, and molecular docking Study. Molecules 25 (10), 2324. https://doi.org/10.3390/molecules25102324.

Takeda, A., Komatsu, T., Nomura, H., Naka, M., Matsuki, N., Ikegaya, Y., Terai, T., Ueno, T., Hanaoka, K., Nagano, T., Urano, Y., 2016. Unexpected photo-instability of 2,6-sulfonamide-substituted BODIPYs and its application to caged GABA. Chem Bio Chem. 17 (13), 1233–1240. https://doi.org/10.1002/cbic.v17.1310.1002/cbic.201600097.

Waghorn, P.A., Jones, M.W., McIntyre, A., Innocenti, A., Vullo, D., Harris, A.L., Supuran, C.T., Dilworth, J.R., 2012. Targeting carbonic anhydrases with fluorescent BODIPY-labelled sulfonamides. Eur J Inorg Chem. 2012 (17), 2898–2907. https://doi.org/10.1002/ejic.v2012.1710.1002/ejic.201101371.

Liu, P., Ma, S., Yan, C., Qin, X., Zhao, P., Li, Q.i., Cui, Y., Li, M., Du, L., 2019. Discovery of small-molecule sulfonamide fluorescent probes for GPR120. Anal Chem. 91 (23), 15235–15239.

Chan, M., Lao, F.S., Chu, P.J., Shpigelman, J., Yao, S., Nan, J., Sato-Kaneko, F., Li, V., Hayashi, T., Corr, M., Carson, D.A., Cottam, H.B., Shukla, N.M., 2019. Structure–activity relationship studies to identify affinity probes in bis-aryl sulfonamides that prolong immune stimuli. J Med Chem. 62 (21), 9521–9540.

Zhao, C., Zhang, J., Wang, X., Zhang, Y., 2013. Pyridone fused boron-dipyrromethenes: synthesis and properties. Org Biomol Chem. 11, 372–377 https://doi:10.1039/C2OB26791H.

Wang, D., Bai, T., Wang, X., Xiong, Y., Zhang, Y., Shi, Z., Zhang, F., Lu, W., Qing, G., 2021. Sensing mechanism of excited-state intermolecular hydrogen bond for phthalimide: indispensable role of dimethyl sulfoxide. Chinese J Chem. 39, 1113–1120. https://doi.org/10.1002/cjoc.202000604.

Zakerhamidi, M.S., Ghanadzadeh, A., Moghadam, M., 2011. Effect of anisotropic and isotropic solvent on the dipole moment of coumarin dyes - ScienceDirect. Spectrochim Acta A. 78 (3), 961–966. https://doi.org/10.1016/j.saa.2010.12.002.

D. Prasannan and C. Arunkumar, A "turn-on-and-off" pH sensitive BODIPY fluorescent probe for imaging E. coli cells. New J Chem. 42 (2018) 3473-82. https://doi:10.1039/c7nj04313a.

Khalil, O.M., Kamal, A.M., Bua, S., El Sayed Teba, H., Nissan, Y.M., Supuran, C.T., 2020. Pyrrolo and pyrrolopyrimidine sulfonamides act as cytotoxic agents in hypoxia via inhibition of transmembrane carbonic anhydrases. Eur J Med Chem. 188, https://doi:10.1016/j.ejmech.2019.112021 112021.

Eldehna, W.M., Nocentini, A., Al-Rashood, S.T., Hassan, G.S., Alkahtani, H.M., Almehizia, A.A., Reda, A.M., Abdel-Aziz, H.A., Supuran, C.T., 2018. Tumor-associated carbonic anhydrase isoform IX and XII inhibitory properties of certain isatin-bearing sulfonamides endowed with in vitro antitumor activity towards colon cancer. Bioorg Chem. 81, 425–432 https://doi:10.1016/j.bioorg.2018.09.007.

Wang, Y., Xiao, F., Shao, T., Hu, K., Lian, G., Feng, J., Chen, H., Jin, G., 2021. A multiple acetal chalcone-BODIPY-based fluorescence: synthesis, physical property, and biological studies. Anal. Bioanal. Chem. 413, 2529–2541 https://doi:10.1007/s00216-021-03208-8.

Ashokkumar, Pichandi, Ashoka, Anila Hoskere, Collot, Mayeul, Das, Amitava, Klymchenko, Andrey S., 2019. A fluorogenic BODIPY molecular rotor as an apoptosis marker. Chem Commun. 55 (48), 6902–6905.

Sun, Yue, Wang, Youwei, Lu, Wenbo, Liu, Chang, Ge, Shengjie, Zhou, Xinyu, Bi, Caili, Cao, Xiaowei, 2021. A novel surface-enhanced Raman scattering probe based on Au nanoboxes for

dynamic monitoring of caspase-3 during cervical cancer cell apoptosis. J Mater Chem B. 9 (2), 381–391.

Zhou, Liyi, Luo, Feijun, Chi, Weijie, Tang, Yiping, Liu, Xiaogang, Lin, Qinlu, 2020. Activatable selenium-containing fluorescent apoptotic agent for biosensing and tracing cancer cell apoptosis. Sens Actuators, B. 311, 127915. https://doi.org/10.1016/j.snb.2020.127915.

Wu, Hong, Chen, Liang, Zhu, Feifei, Han, Xu, Sun, Lindan, Chen, Keping, 2019. The cytotoxicity effect of resveratrol: Cell cycle arrest and induced apoptosis of breast cancer 4T1 cells. Toxins. 11 (12), 731. https://doi.org/10.3390/toxins11120731.

Yang, Nian, Li, Chen, Li, Hongliang, Liu, Ming, Cai, Xiaojun, Cao, Fengjun, Feng, Yibin, Li, Minglun, Wang, Xuanbin, 2019. Emodin induced SREBP1-dependent and srebp1-independent apoptosis in hepatocellular carcinoma cells. Front Pharmacol. 10. https://doi.org/10.3389/fphar.2019.00709.

Chen, Zhenghu, Wang, Zhenyu, Pang, Jonathan C., Yu, Yang, Bieerkehazhi, Shayahati, Lu, Jiaxiong, Hu, Ting, Zhao, Yanling, Xu, Xin, Zhang, Hong, Yi, Joanna S., Liu, Shangfeng, Yang, Jianhua, 2016. Multiple CDK inhibitor dinaciclib suppresses neuroblastoma growth via inhibiting CDK2 and CDK9 activity. Sci Rep. 6 (1). https://doi.org/10.1038/srep29090.

Shao, Hao, Foley, David W., Huang, Shiliang, Abbas, Abdullahi Y., Lam, Frankie, Gershkovich, Pavel, Bradshaw, Tracey D., Pepper, Chris, Fischer, Peter M., Wang, Shudong, 2021. Structure-based design of highly selective 2,4,5-trisubstituted pyrimidine CDK9 inhibitors as anti-cancer agents. Eur J Med Chem. 214, 113244. https://doi.org/10.1016/j.ejmech.2021.113244.

Alnoman, Rua B., Hagar, Mohamad, Parveen, Shazia, Ahmed, Hoda A., Knight, Julian G., 2020. Computational and molecular docking approaches of a New axially chiral BODIPY fluorescent dye. J Photochem Photobiol, A. 395, 112508. https://doi.org/10.1016/j.jphotochem.2020.112508.

Shi, Tong, Xiong, Zhiyu, Jin, Wengang, Yuan, Li, Sun, Quancai, Zhang, Yuhao, Li, Xiuting, Gao, Ruichang, 2020. Suppression mechanism of l-arginine in the heat-induced aggregation of bighead carp (Aristichthys nobilis) myosin: The significance of ionic linkage effects and hydrogen bond effects. Food Hydrocolloids. 102, 105596. https://doi.org/10.1016/j.foodhyd.2019.105596.